NASA TECHNICAL NOTE

NASA TN D-2876

EXPERIMENTAL INVESTIGATION OF BLAST LOADING ON AN AIRFOIL IN MACH 0.7 AIRFLOW WITH INITIAL ANGLE-OF-ATTACK CHANGE OF 28°

by James C. Manning

Langley Research Center

Langley Station, Hampton, Va.

NATIONAL AERONAUTICS AND SPACE ADMINISTRATION • WASHINGTON, D. C. • JUNE 1965

NASA TN D-2876

EXPERIMENTAL INVESTIGATION OF BLAST LOADING ON AN AIRFOIL IN MACH 0.7 AIRFLOW WITH INITIAL ANGLE-OF-ATTACK CHANGE OF 28°

By James C. Manning

Langley Research Center
Langley Station, Hampton, Va.

NATIONAL AERONAUTICS AND SPACE ADMINISTRATION

For sale by the Clearinghouse for Federal Scientific and Technical Information
Springfield, Virginia 22151 – Price $1.00

EXPERIMENTAL INVESTIGATION OF BLAST LOADING ON AN AIRFOIL IN MACH 0.7 AIRFLOW WITH INITIAL ANGLE-OF-ATTACK CHANGE OF 28°

By James C. Manning
Langley Research Center

SUMMARY

An experimental investigation has been completed to examine the blast loading imposed on an airfoil in Mach number 0.7 flow by a blast wave which caused an initial change in angle of attack of approximately 28°. Pressure distributions along one chord of the airfoil at intervals of 0.1 millisecond show the initial diffraction of the blast wave around the airfoil, whereas subsequent distributions at intervals of 0.5 millisecond show the progress along the chord of a leading-edge vortex formed in the diffraction period. Normal-force coefficients obtained from the pressure distributions were substantially greater than those from a wind-tunnel investigation, but were well correlated with those from a previous blast-loading investigation at an initial angle-of-attack change of 18.8°.

INTRODUCTION

Information on blast loading imposed on aircraft is important in avoiding damage to aircraft delivering nuclear weapons and in determining the lethal envelope about aircraft subjected to nuclear antiaircraft weapons. Although analytical studies of blast-loading conditions have provided a basis for operational planning, the very complex loading conditions that accompany the diffraction of blast waves around aircraft wings can best be defined in the subsonic region by the use of experimental investigations. To provide an experimental approach to the blast-loading problem, a series of tests were conducted with the ground blast apparatus at the NASA Wallops Station to investigate the loading imposed on a 45° sweptback model wing immersed at zero angle of attack in a Mach 0.7 airflow and subjected to a blast wave that caused an initial change in angle of attack well beyond the steady-stall angle of the wing section. The results from the first series of tests are given in reference 1 for an initial change in angle of attack of 18.8°. This paper extends the results of reference 1 to an initial change in angle of attack of about 28°. The data are presented in the form of pressure distributions along a single midsemispan chord of the model wing.

SYMBOLS

a_1	ambient speed of sound, ft/sec
c	airfoil-section chord
C_m	pitching-moment coefficient about quarter-chord station
C_N	normal-force coefficient
g	acceleration due to gravity, ft/sec^2
M	Mach number
p	local pressure measured along chord, lb/sq in.
p_1	ambient pressure (ahead of shock front), lb/sq in.
p_2	faired side-on overpressure, lb/sq in.
p/q	load coefficient
q	stream dynamic pressure, lb/sq in.
t	time after blast-wave arrival, msec
U	shock velocity, ft/sec
V	airstream velocity, ft/sec
V_b	blast-induced gust velocity, ft/sec
α	angle of attack, deg
γ	ratio of the specific heats of air
ρ_1	ambient density, slug/ft^3
ρ_2	density of air behind the shock front, slug/ft^3

APPARATUS AND TESTS

Test Configuration

The blast tests simulated an airplane in level flight being struck by a blast wave originating from below and normal to the flight path. The airplane

is assumed to be flying at $M = 0.7$ and to be subjected to a blast wave that would cause an angle-of-attack change of approximately 28°. The procedure used in the simulation of these conditions with the ground blast apparatus is illustrated by the schematic diagram of figure 1. The plane of the test has been rotated 90° by rolling the model until its wings are vertical and the explosion is placed to one side of the model so that the blast wave still strikes the bottom of the model. The forward flight of the airplane is simulated by subjecting the model to $M = 0.7$ airflow from the shock tunnel.

Model

The geometric details and a photograph of the model used in these tests as well as in the tests of reference 1 are shown in figures 2 and 3, respectively. The model wing had an NACA 65A006 airfoil section parallel to the plane of symmetry and had the quarter-chord line swept back 45°. The wing of the model was instrumented along the midsemispan chord with flush-diaphragm pressure gages (of the type used in the tests of ref. 1) on both surfaces at 13 matching stations. However, only 12 recording channels of instrumentation were available for pressure measurements along the wing chord. Therefore, four channels were used with gages located at 5.0-, 22.5-, 52.5-, and 92.5-percent wing chord to define the chordwise pressure distribution on the wing surface facing the blast (designated the "blast side"). The remaining eight channels were used with selected gages on the surface away from the blast (designated "lee side") to define the more complex chordwise pressure distribution on this surface of the wing. The locations selected on the lee side were 2.5, 5.0, 7.5, 15.0, 32.5, 52.5, 86.0, and 92.5 percent of the wing chord. The model also had a probe that extended forward from the nose of the fuselage (fig. 3) and measured the total pressure and the static pressure of the airstream prior to the arrival of the blast wave.

Instrumentation

The pressure measurement system used in this investigation was developed at the Langley Research Center for the measurement of transient pressures encountered in shock-tube and blast-effect research. The system capabilities and a detailed description of the system are presented in reference 2. The pressure-measurement system, which is basically composed of miniature flush-diaphragm inductance gages, a companion 120-kilocycle carrier amplifier system, commercial dual-beam oscilloscopes, and NASA 70-mm strip cameras, has a frequency response which was flat up to 20 kilocycles. Within the pressure range of -15 to 30 lb/sq in. which is typical for the wing gages, the system has a linearity within approximately ± 1.5 percent of full scale. Since the initial acceleration due to the blast was expected to be approximately 100g units, the gage output due to acceleration was determined both theoretically and experimentally and was found to be approximately 0.2 percent of full scale per 100g units.

A blast gage, consisting of a miniature inductance gage embedded in a small brass disk, was used to measure the side-on or static overpressures

created by the blast. It was located in the tunnel flow on the model support just rear of the model wing. (See figs. 1 and 3.) The methods of amplification and recording are identical to those used for the wing gages.

Explosive Charge

The explosive charge, an aluminized explosive mixture (HBX-1) cast in a hemispherical shape, weighed approximately 650 pounds. The charge was located on a wooden tower about 12 feet above the ground and 90 feet from the model in a plane perpendicular to the tunnel airflow over the model. By placing the charge in this manner, the model and tunnel airstream were in Mach stem region (see ref. 3) and were hence subjected to a single shock front.

Shock Tunnel

The shock tunnel of the ground blast apparatus, which is described in reference 1, is essentially a blowdown tunnel with a diaphragm used as a quick opening valve. It is 10 feet in diameter and has a pressurized section 80 feet long. Heaters are provided in the pressurized section so that upon diaphragm rupture the air expands isentropically to atmospheric pressure and temperature. Therefore, the airflow over the model has the same density as the surrounding still air, and thus the interference to the blast wave as it passes through the tunnel airstream toward the model is minimized. The tunnel is capable of producing steady flow at Mach 0.7 for a period of 50 to 70 milliseconds in duration.

Blast-Wave Measurements

The actual blast-wave conditions in the tunnel airflow were measured by the blast gage positioned rear of the model wing and oriented to measure side-on or static overpressure in the blast wave. Time histories of the side-on overpressure for each test are given as the solid lines in figure 4. The character of the fine detail of these time histories as well as that of subsequently presented histories is different from that of reference 1 because of a change in readout procedure. In reference 1, each discernible feature of the photographic records was read along with its time. In the present paper, the readout procedure was simplified by taking readings at set time intervals; thus, such features as the high-frequency oscillations shown at the beginning of the blast-wave overpressure time histories of reference 1 were filtered out, but the photographic record was adequately represented.

The pressure time histories of figure 4 (solid lines) were faired as shown by the dashed lines, and these fairings were used in a subsequent analysis to represent the blast-wave conditions. As in reference 1, the pressure spike (at about 1.5 milliseconds) attributed to the effect of the passage of the blast wave through the mixing zone surrounding the steady air stream as well as the subsequent low-frequency-pressure oscillation believed to be caused by location of the blast gage in the wake of the wing are disregarded in the fairings.

Test Conditions

The initial test conditions at blast-wave arrival at the model were as follows:

	Test 1	Test 2
Airstream velocity, V, ft/sec	742	798
Airstream Mach number, M	0.675	0.712
Blast-wave overpressure, lb/sq in.	9.10	9.99
Induced gust velocity, V_b, ft/sec	389	427
Angle-of-attack change, $\Delta\alpha$, deg	27.7	28.1
Atmospheric temperature, ^{o}F	45	54
Atmospheric pressure, lb/sq in.	14.80	14.92
Dynamic pressure, q, lb/sq in.	8.36	9.92
Distance from model to blast, ft	90	90

The time histories of the induced gust velocities were determined by the Rankine-Hugoniot shock-wave relations as shown below and the faired side-on blast-wave overpressure measurements. Although the Rankine-Hugoniot shock-wave relations define the blast-wave characteristics at the shock front, the relations were also used to obtain a good approximation of the induced gust velocity and density subsequent to the initial shock. The change in angle of attack (fig. 5) was determined by the vector addition of the induced gust velocity and the airstream velocity. The dynamic pressure was obtained by use of the relative-velocity vector determined by the vector addition and the calculated values of the density of the airstream during the overpressure period. The Rankine-Hugoniot relations used to determine the induced gust velocity and the density, respectively, are as follows:

$$V_b = \frac{a_1 p_2}{\gamma p_1}\left(1 + \frac{(\gamma + 1)p_2}{2\gamma p_1}\right)^{-1/2}$$

$$\rho_2 = \rho_1 \frac{2\gamma p_1 + (\gamma + 1)p_2}{2\gamma p_1 + (\gamma - 1)p_2}$$

RESULTS AND DISCUSSION

Time Histories of Pressure on Wing Chord

Time histories of the pressure changes on the airfoil for tests 1 and 2 are plotted in figures 6(a) and 6(b) at each active gage location. Each history is plotted so that time increases with distance away from the airfoil, zero time being the instant that the blast wave strikes the side of the airfoil facing the blast. The pressure scale shown in the lower left of the

figure is common to all histories. (Care must be taken to aline the zero axis with the percent-chord line for each reading.) At the upper left of each figure, the initial directions of the airflow and the blast wave are shown. The dashed curve labeled blast gage, plotted with each blast-side pressure history, is the faired pressure history of the side-on blast-wave overpressure measurements shown in figures 4(a) and 4(b).

This investigation involved such severe wing loadings that some instrumentation difficulty was experienced. In test 1 ($\Delta\alpha = 27.7^{\circ}$), the wing gages located at 2.5-, 32.5-, and 52.5-percent chord on the lee side malfunctioned after 6, 7, and 8 milliseconds, respectively. Also, the pressure measurement made at 52.5-percent chord on the blast side was suspiciously low during the test; thus, there may have been an error in calibration of the gage. Despite repair attempts, the same lee-side gages that malfunctioned in test 1 malfunctioned in test 2. Hence, the measurements at these stations were not included in figure 6(b).

Comparison of the wing-pressure time histories measured in each test, figures 6(a) and 6(b), shows that the pressure histories are similar in shape. This similarity is especially evident in the pressure histories measured on the blast side of the wing; however, there is a difference, primarily in the fine detail, in the pressure histories on the lee side. In both tests, the major pressure changes along the chord follow the same sequence.

The pressure time histories on the blast side of the airfoil jump almost instantaneously to a pressure value of 2 to $2\frac{1}{2}$ times the initial side-on pressure measured by the blast gages (dashed lines). These results are representative of the ratio of reflected to side-on pressure measurements made in free air at this pressure level. As pointed out in reference 1, the airflow over the wing tends to retain the pressure over the forward portion of the wing and causes this pressure to reduce more quickly toward the trailing edge of the airfoil; as a result, the center of pressure of the airfoil, which is initially at the 50-percent-chord station, moves forward as a function of time.

The progress of the blast-wave diffraction around the wing of the model was indicated by the arrival of the first pressure signal at each active gage location on the lee side. A plot of the diffraction about the wing for test 1 is shown in figure 7, in which the circles represent the measured arrival time of the first pressure signal at the gage stations. As might be expected, the airflow causes an unsymmetrical diffraction of the blast wave around the leading and trailing edges. In figure 7, the broken line and the dotted line represent an estimation of the diffraction about the leading and the trailing edges of the wing, respectively, calculated by the method described in reference 1. Briefly, this method took into account the average local airstream velocity over the wing chord and the estimated velocity of the diffracting wave in still air. It was assumed that the still-air blast-wave velocity was a function of the maximum average positive pressure measured at the lee-side wing gages as the wave passed over these gages from the 2.5- to the 52.5-percent-chord stations for the portion of the wave diffracting from the leading edge and from the 92.5- to the 86-percent-chord stations for the portion diffracting from the trailing edge.

However, it appears that a simpler solution can be used to estimate the wave propagation about the wing with acceptable precision. This method, which is represented in figure 7 by the solid and dashed lines, combines the free-stream velocity with the calculated still-air diffracting-blast-wave velocity based on the maximum side-on blast-wave overpressure measured in the airstream. In this particular case, there was not a significant difference in the diffraction around the trailing edge between the two methods used in the diffraction calculations. In both cases, the still-air velocity of the diffracting blast wave was estimated by using the Rankine-Hugoniot relation for a single shock front as follows:

$$U = a_1\left(1 + \frac{(\gamma + 1)p_2}{2\gamma p_1}\right)^{1/2}$$

Pressure Distributions on Wing Chord

Pressure distributions along the wing chord for test 1 were constructed for 0.1-millisecond intervals from 0 to 0.5 millisecond and for 0.5-millisecond intervals from 0.5 to 6.5 milliseconds after the blast wave arrived at the wing. The values used in the pressure distribution were determined by fairing the pressure time histories of figure 6(a) as indicated by the samples for the blast and lee sides shown in figures 8 and 9, respectively. The pressures read from the faired histories at the indicated times were divided by the dynamic pressure q occurring at the corresponding times and plotted at the gage locations. The resulting pressure distributions are presented in figure 10 for the times and the associated instantaneous angles of attack after blast-wave arrival.

Since the pressure time histories in figure 6(a) are referenced to the pressures at the measuring stations prior to the arrival of the blast wave, the pressure distributions are also referenced to these same ambient conditions prior to blast-wave arrival. This reference is unrealistic from an aerodynamic point of view; therefore, the horizontal broken line was included to show the instantaneous static ambient pressure determined by dividing the instantaneous side-on, or static, overpressure by the corresponding dynamic pressure. The pressure coefficient located at 52.5-percent chord on the blast side of the wing was ignored in the fairing of each distribution because, as previously indicated, it was believed that this pressure gage malfunctioned during the test. Construction of pressure distributions for test 2 was not practical because of insufficient pressure data due to instrumentation malfunctions occurring during the tests.

In the first 0.5 millisecond (figs. 10(a) to 10(f)), the diffraction of the blast wave around the wing is illustrated. At zero time, the blast wave has just struck the blast side of the wing; subsequently, at 0.1 millisecond, it has moved or diffracted around the leading and trailing edges of the wing to the lee side as indicated by the increased values of p/q. The dashed lines estimate the further progress of the wave toward the next station. Shortly after 0.5 millisecond (fig. 10(f)), the diffraction about the wing is complete.

The first evidence of a negative pressure developing and indicating the formation of a vortex appears at 0.1 millisecond (fig. 10(b)) where the pressure at 2.5-percent chord (lee side) is almost zero, whereas a positive pressure exists at the 5-percent-chord station. This indication appears about 0.1 millisecond earlier than it appears in reference 1, but the difference is probably a result of making the first pressure measurement at the 2.5-percent-chord station rather than at the 5-percent-chord station as was done in reference 1. In a comparison of the pressure distributions of these tests with the tests of reference 1, it can be seen that the pressure level at the 5-percent-chord station is about equal in both cases; this equality gives further proof of the earlier occurrence of the vortex. From 0.2 to 0.5 millisecond, the negative pressure associated with the vortex has developed and increased in magnitude and intensity. The negative peak associated with the movement of the vortex along the chord is clearly shown in figures 10(c) to 10(l), 0.5 millisecond to 3.5 milliseconds. Over this time interval of 0 to 3.5 milliseconds, the pressure distributions on the lee side of the airfoil for these tests and reference 1 are very similar in shape. However, the remainder of the pressure distributions along the lee side (figs. 10(m) to 10(r), which show the after-effects on the flow of the rapidly decreasing angle of attack) have strong peaks which are not present in reference 1 at both the leading and the trailing edges of the airfoil. Despite the rapidly changing shapes of the pressure distributions on the lee side of the wing, the distributions on the blast side are regular in shape and decrease in an orderly manner after the initial pressure is imposed on the airfoil. The shapes of these distributions are also similar to those of reference 1.

Loads and Moments on Wing Chord

Normal-force coefficients of the wing section, obtained by integration of the pressure distributions of figure 10, are shown in figure 11 as a function of their corresponding instantaneous angle-of-attack values. Also included in the figure are the variations in the normal-force coefficients from the test data of reference 1 (the circles) between 8.5° and 18.8° and the steady-flow variation of the normal-force coefficients derived from the wind-tunnel data of reference 4 (the dashed line) between 0° and 20°. Upon examination of the figure, it can be seen that the initial blast loading (at 27.7°) obtained during this investigation is almost three times the maximum steady-flow variation of reference 4 and approximately 50 percent greater than the initial blast loading (at 18.8°) of reference 1. This difference, of course, represents an approximately linear increase in the variation of initial loading with initial angle-of-attack change as indicated by the broken line originating at zero and passing through these points. The subsequent history of the normal-force coefficient for the present test from the initial point at 27.7° to the limit of the usable data at 19.1° is well above the maximum steady-flow normal-force coefficient obtained from the wind-tunnel investigation of reference 4.

Further examination of figure 11 shows that the first part of the history between 27.7° and 23.9° is nearly identical in shape to the first part of the history from reference 1 between 18.8° and 15.7°. Downward from these points of 23.9° and 15.7°, the curves from reference 1 deviate from the curves of the present test which immediately reduce toward zero approximately in proportion

to the reduction in angle of attack, whereas for the data of reference 1, the load coefficient first increases considerably before reducing toward zero. It is believed in the present case that the angle of attack may be too high to permit full development of lift and that, after $1\frac{1}{2}$ chord lengths (23.9°), some separation of the flow is present on the wing section; this separation indicates partial stalling.

To emphasize the blast loading on the wing and the possibility of wing-section stall in the latter part of the test, the normal-force coefficients of test 1 and reference 1 are shown in figure 12 as a function of airflow over the wing in chord lengths. The solid lines represent the total values, and the dashed lines show the portion of the coefficient values resulting from the pressure increment imposed on the blast side of the wing as referenced to the airstream static pressure prior to the blast-wave arrival. The difference between the solid and dashed curves represents the pressures generated on the lee side of the wing. In both investigations for about the first one-half chord length, it is apparent that the loading is almost entirely produced on the blast side of the wing; the positive pressures on the lee side during this initial diffraction period actually reduce the coefficients. After the first one-half chord length negative pressures develop on the lee side of the wing and add to the loading imposed on the blast side of the wing. Comparison of the curves of the present test with those of reference 1 shows that the loading increased with the additional 9° increase in angle of attack and remained well above that obtained in the previous investigation of an 18.8° angle-of-attack change for almost three chord lengths of airflow. The comparison also shows that the relative contribution of the negative pressures to the total in the present test is considerably less than that shown for reference 1 and, in addition, appears to be less steady. This comparison lends further strength to the belief that the wing section may be partially stalled in the present case.

In figure 13, the pitching-moment coefficients about the quarter chord of the airfoil are plotted as a function of the corresponding instantaneous angle of attack. These coefficients are also compared with those of references 1 and 4. It is obvious that the pitching moments of this investigation are similar in shape to those of reference 1, but are considerably larger initially. Likewise, these moments are much greater than those of the steady-flow wind-tunnel test. The initial peak of $C_m = -7$ at 27.7° is caused by the almost rectangular pressure distribution along only the blast side of the airfoil, figure 10. As the vortex begins to form at the leading edge, the coefficients drop rapidly and only start to increase again when the vortex moves back along the chord. The second general decrease, which is more gradual than the first, is influenced by the fact that the pressure along the blast side of the airfoil becomes lower at the trailing edge than at the leading edge.

CONCLUDING REMARKS

The results of an experimental investigation of blast loading imposed on an airfoil in Mach 0.7 flow by a blast wave which instantaneously changed the

angle of attack from 0° to 27.7° show that the resultant load and pitching-moment coefficients are considerably greater than those obtained in a steady-flow wind-tunnel investigation. This experiment, which gives good qualitative correlation with a previous examination for an initial angle-of-attack change from 0° to 18.8°, shows that the loading increased with the additional 9° increase in angle of attack and remained well above that obtained in the previous investigation of an 18.8° angle-of-attack change for almost three chord lengths of airflow. It appears that the increased loading in this investigation is primarily due to the increase in loading on the blast side of the airfoil. In addition, after about $1\frac{1}{2}$ chord lengths, it appears that the airflow over the wing section is beginning to separate and cause partial stalling of the wing section.

Langley Research Center,
National Aeronautics and Space Administration,
Langley Station, Hampton, Va., March 24, 1965.

REFERENCES

1. Pierce, Harold B.; and Manning, James C.: Experimental Investigation of Blast Loading on an Airfoil in Mach Number 0.7 Airflow With Initial Angle-of-Attack Change of 20°. NASA TN D-1603, 1963.

2. Morton, Richard W.; and Patterson, John L.: A Transient Pressure Measurement System for Blast Effect Research. 1961 Proc. ISA 16th Annual Instrument-Automation Conf. and Exhibit, vol. 16-pt. 2-a, 1961, pp. 148-LA-61-1 - 148-LA-61-16.

3. Glasstone, Samuel, ed.: The Effects of Nuclear Weapons. Rev. ed., U.S. At. Energy Comm., Apr. 1962.

4. Loving, Donald L.; and Williams, Claude V.: Aerodynamic Loading Characteristics of a Wing-Fuselage Combination Having a Wing of 45° Sweepback Measured in the Langley 8-Foot Transonic Tunnel. NACA RM L52B27, 1952.

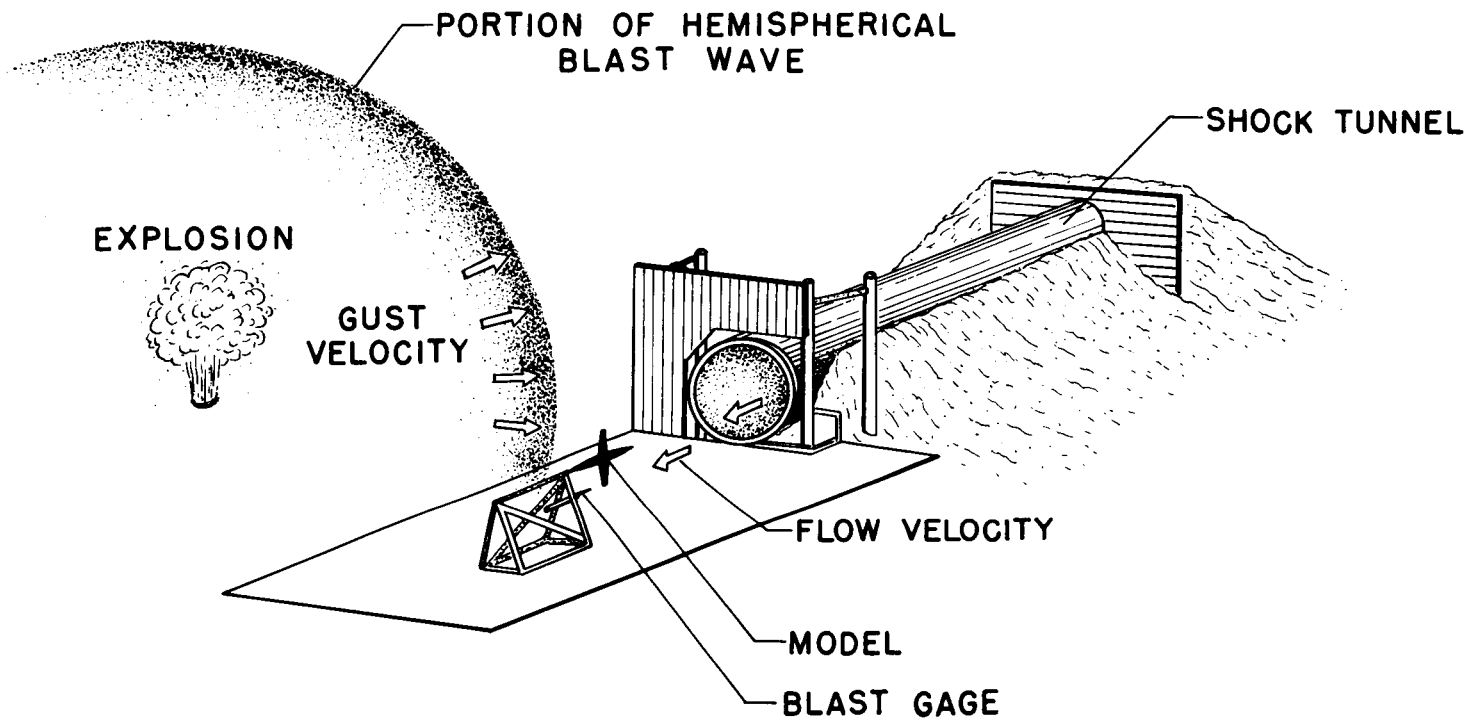

Figure 1.- Blast research with fixed model.

Wing Details

Taper	0.6
Aspect ratio	4.0
Wing area, sq ft	9
Incidence, deg	0
Dihedral, deg	0
Geometric twist	0
Airfoil section	NACA 65A006 (parallel to plane of symmetry)

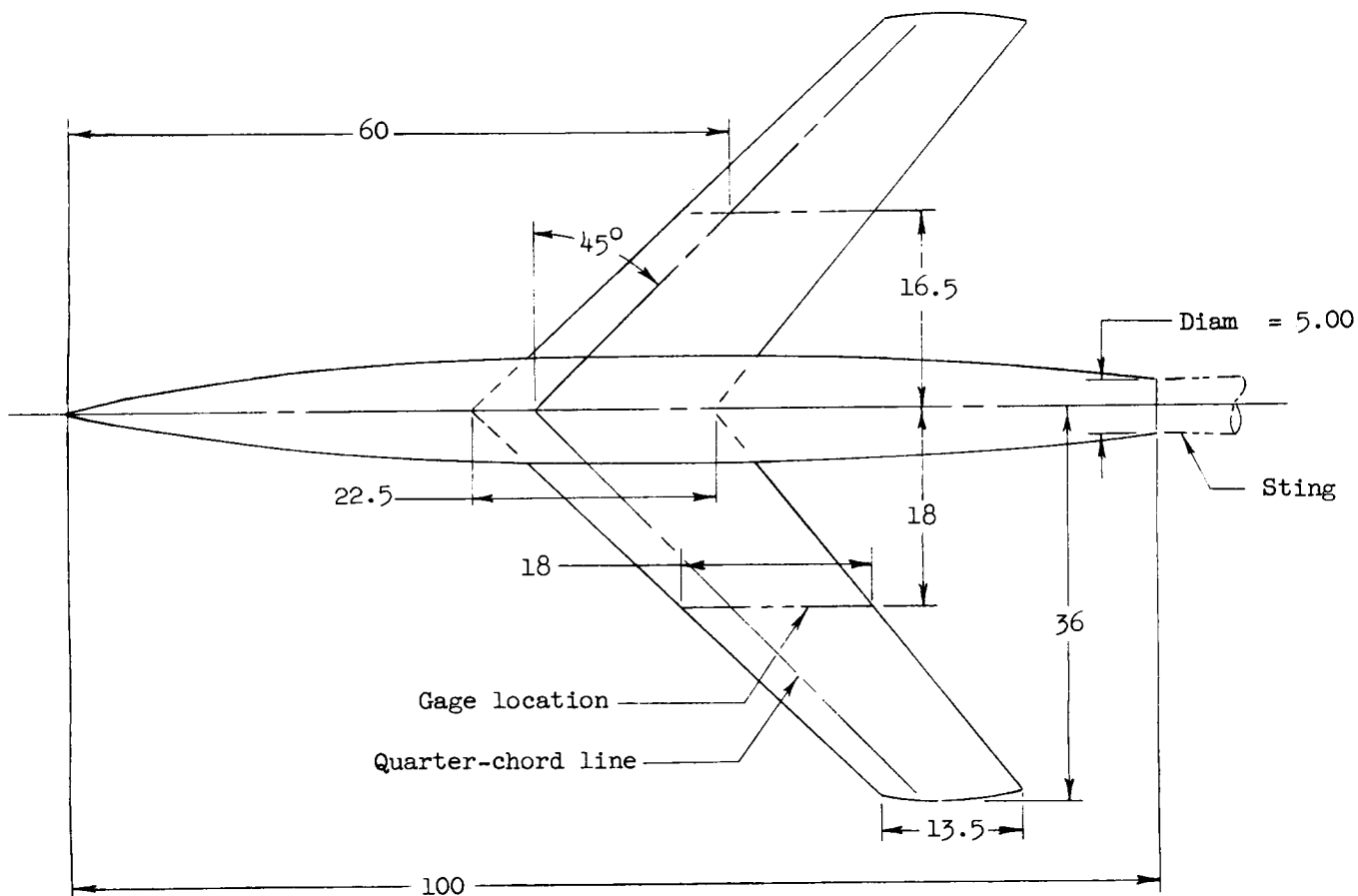

Figure 2.- Model details. All dimensions are in inches.

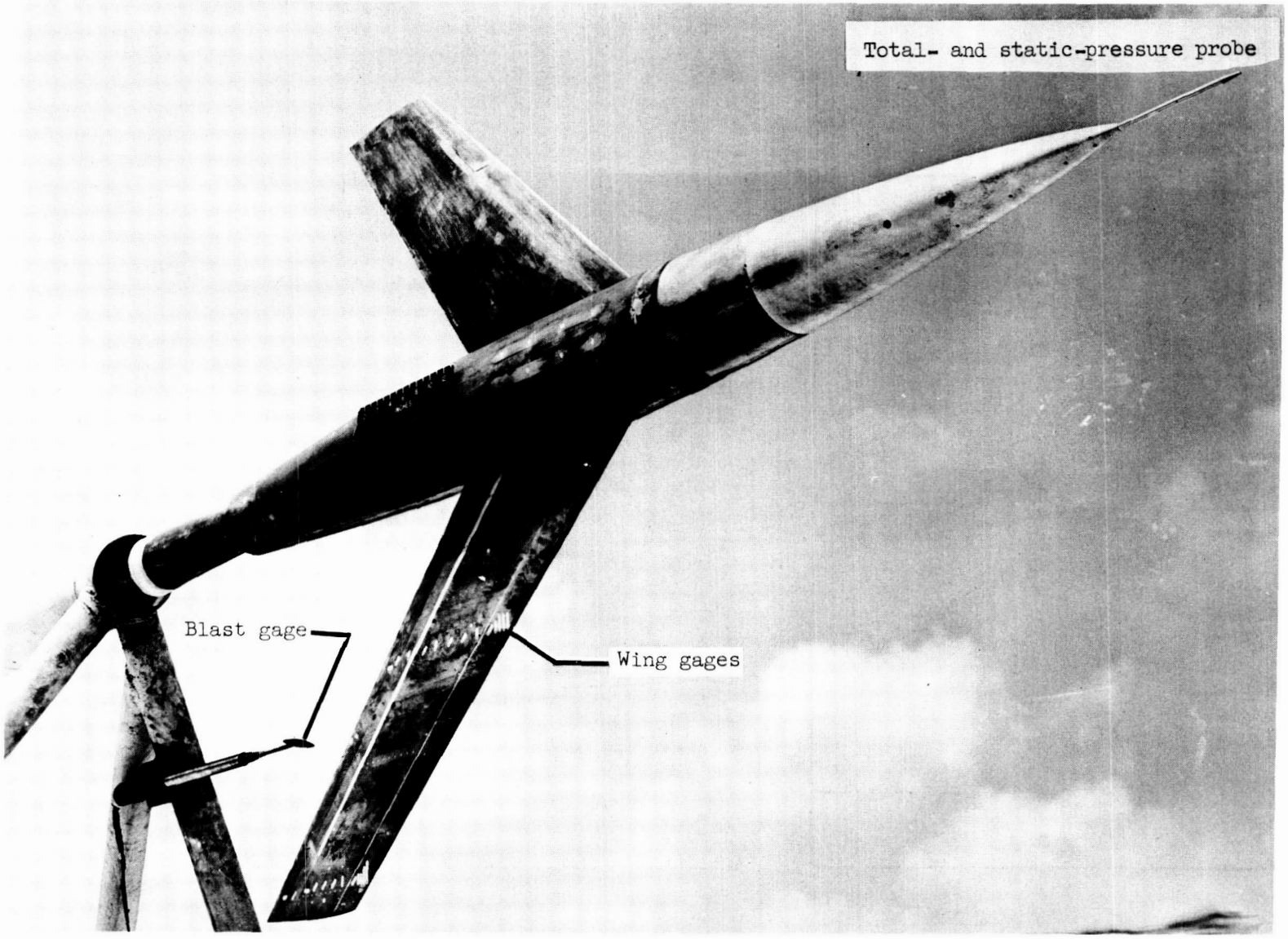

Figure 3.- Photograph of model.

L-60-5852.1

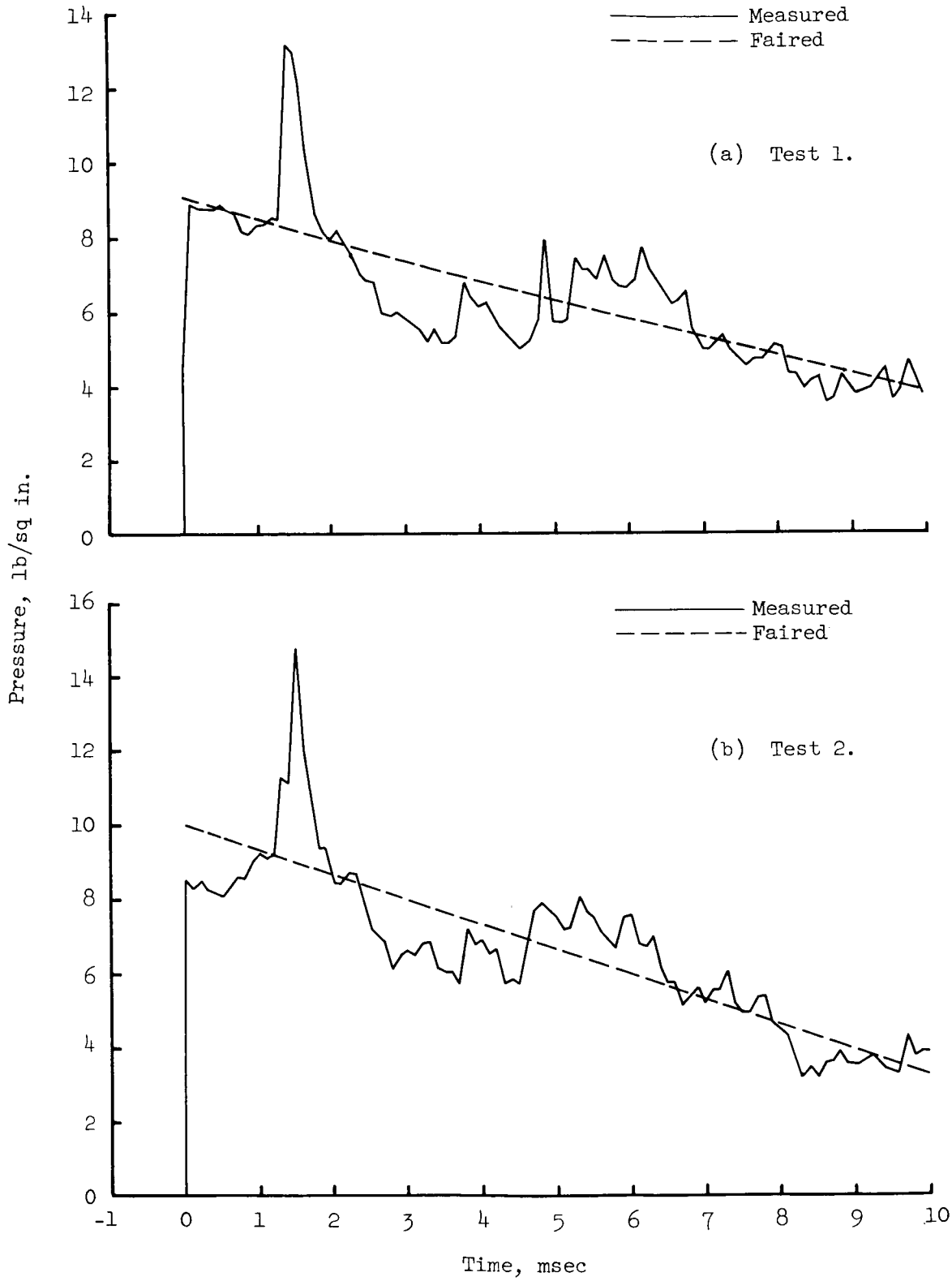

Figure 4.- Overpressure time histories of blast gages.

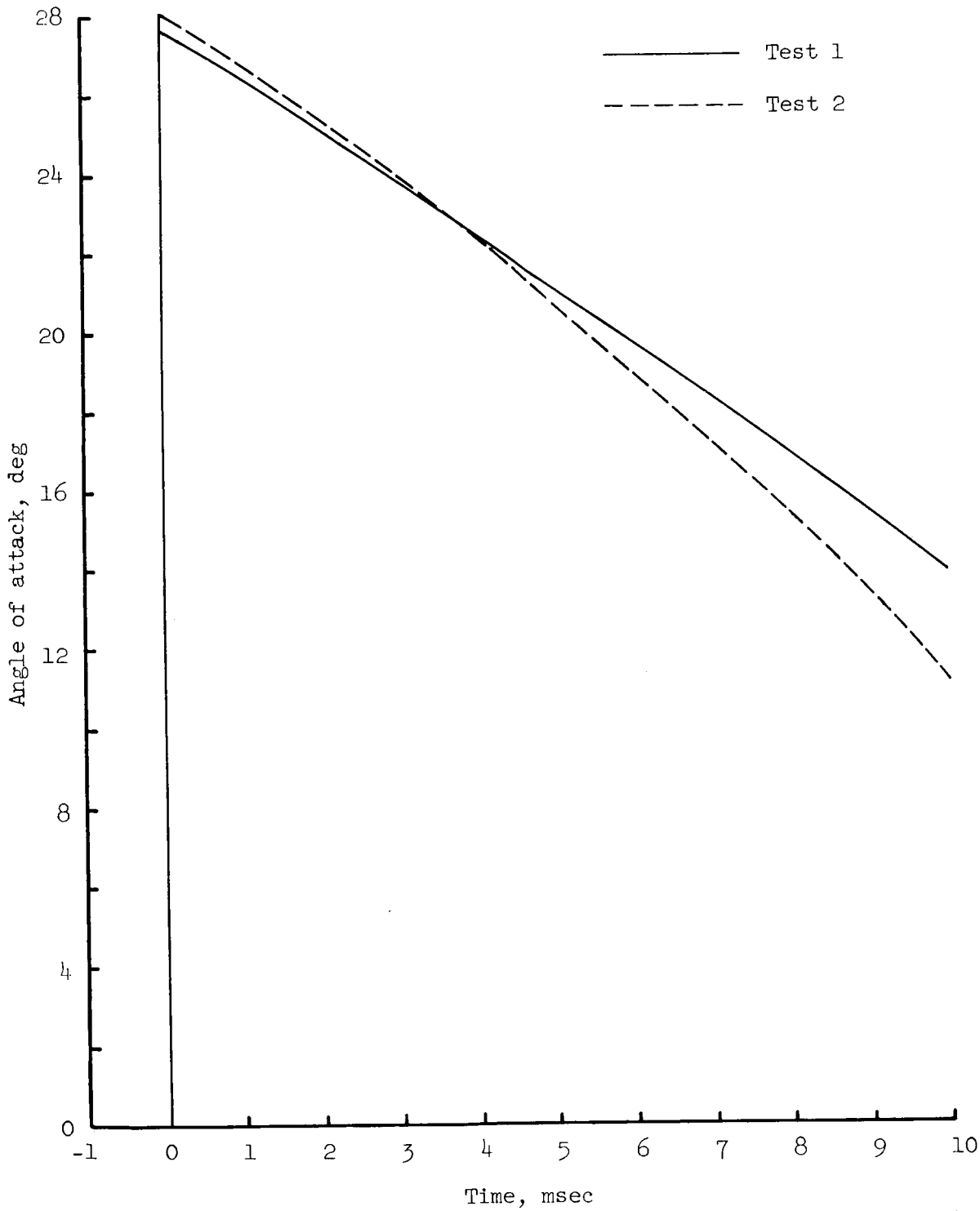

Figure 5.- Angle-of-attack variations.

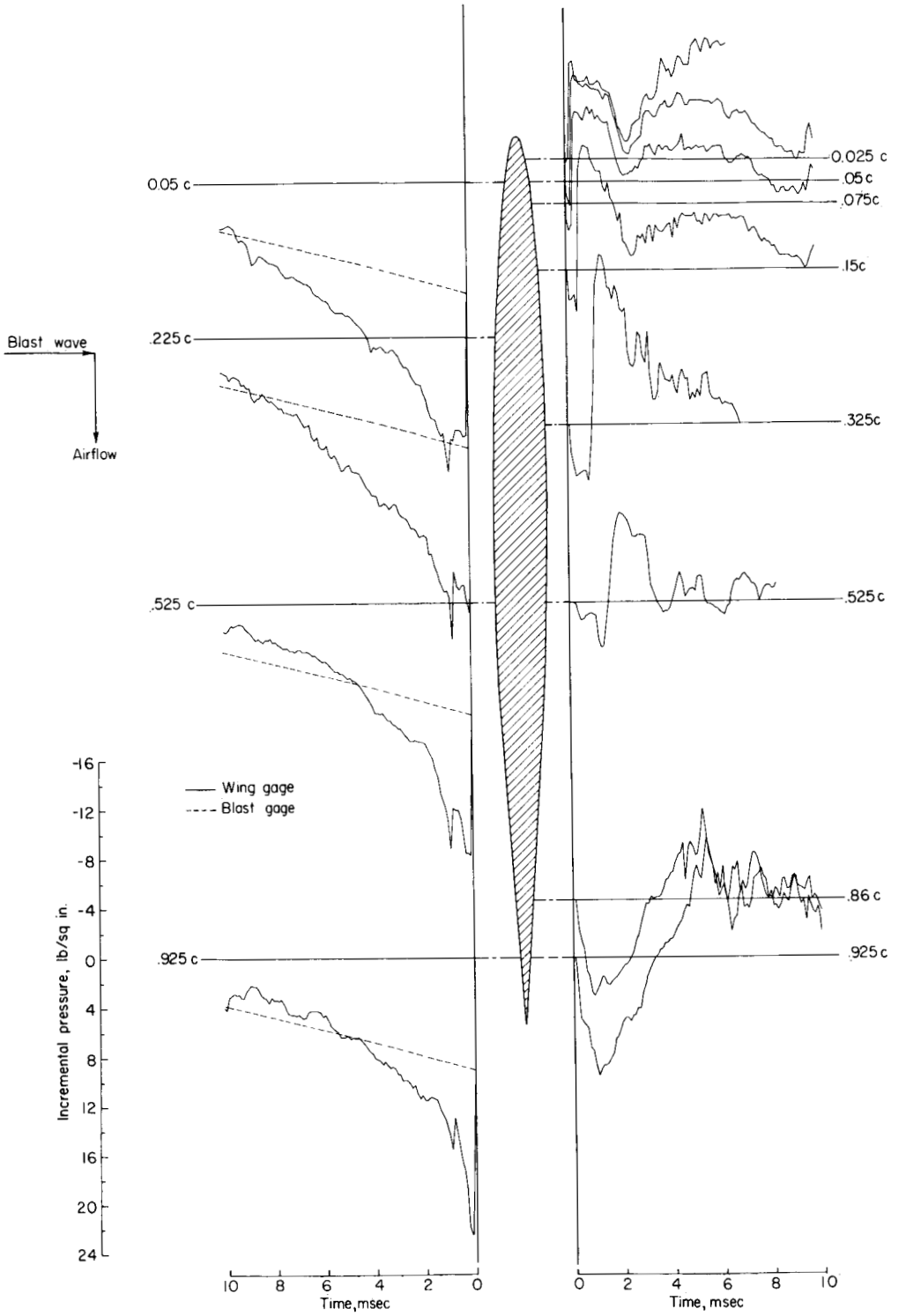

(a) Test 1. $\Delta\alpha = 27.7^{\circ}$.

Figure 6.- Pressure time histories on wing chord. (Care must be taken to aline the zero axis with the percent-chord line for each reading.)

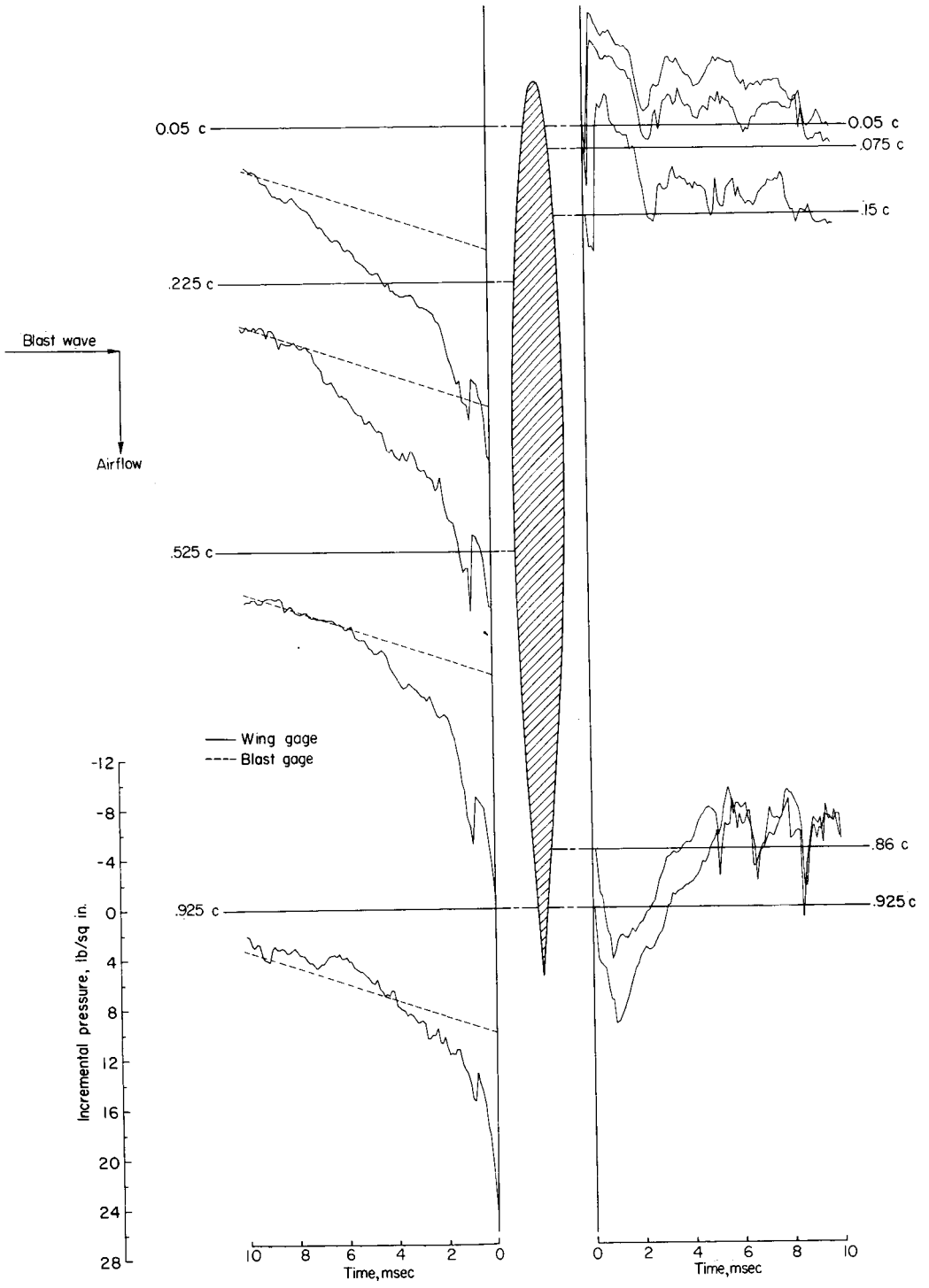

(b) Test 2. $\Delta\alpha = 28.1^{\circ}$.

Figure 6.- Concluded.

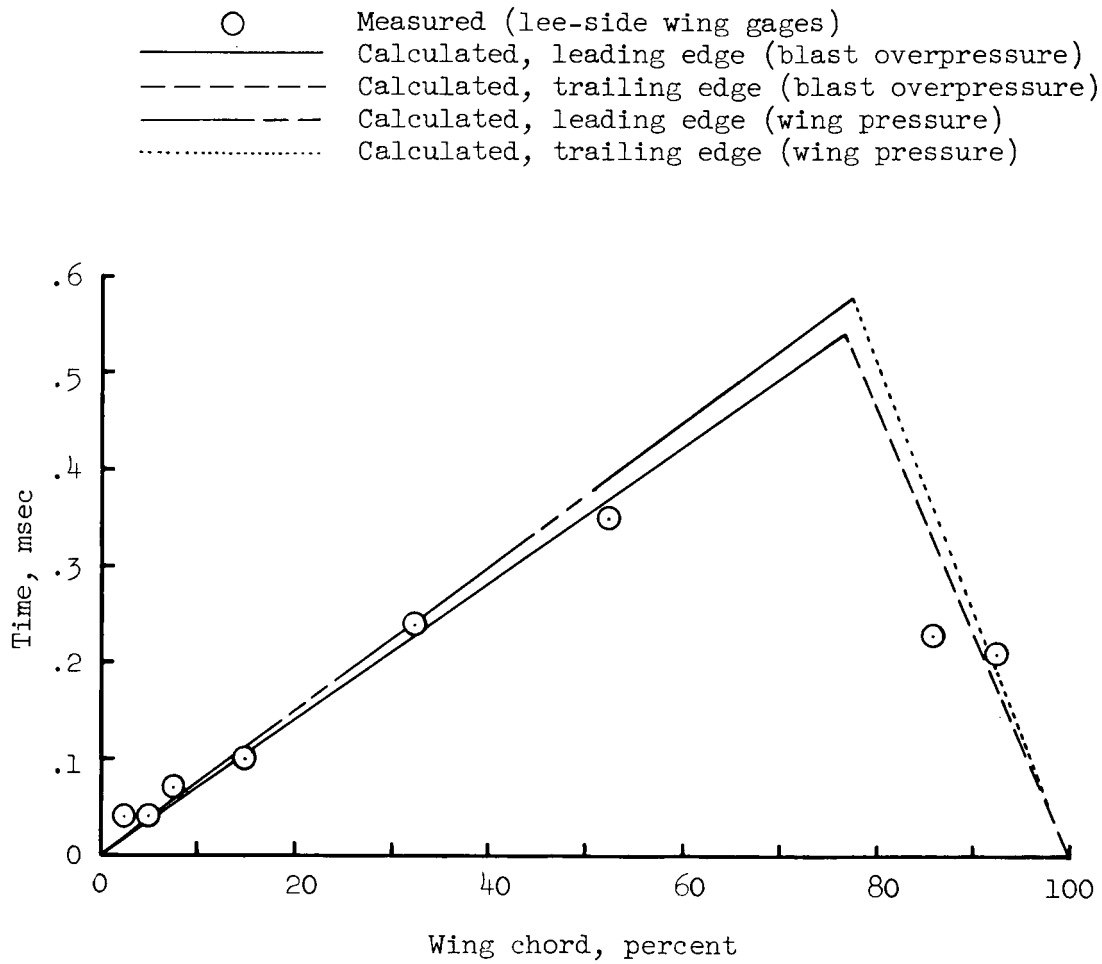

Figure 7.- Diffraction of blast wave. Test 1; lee side.

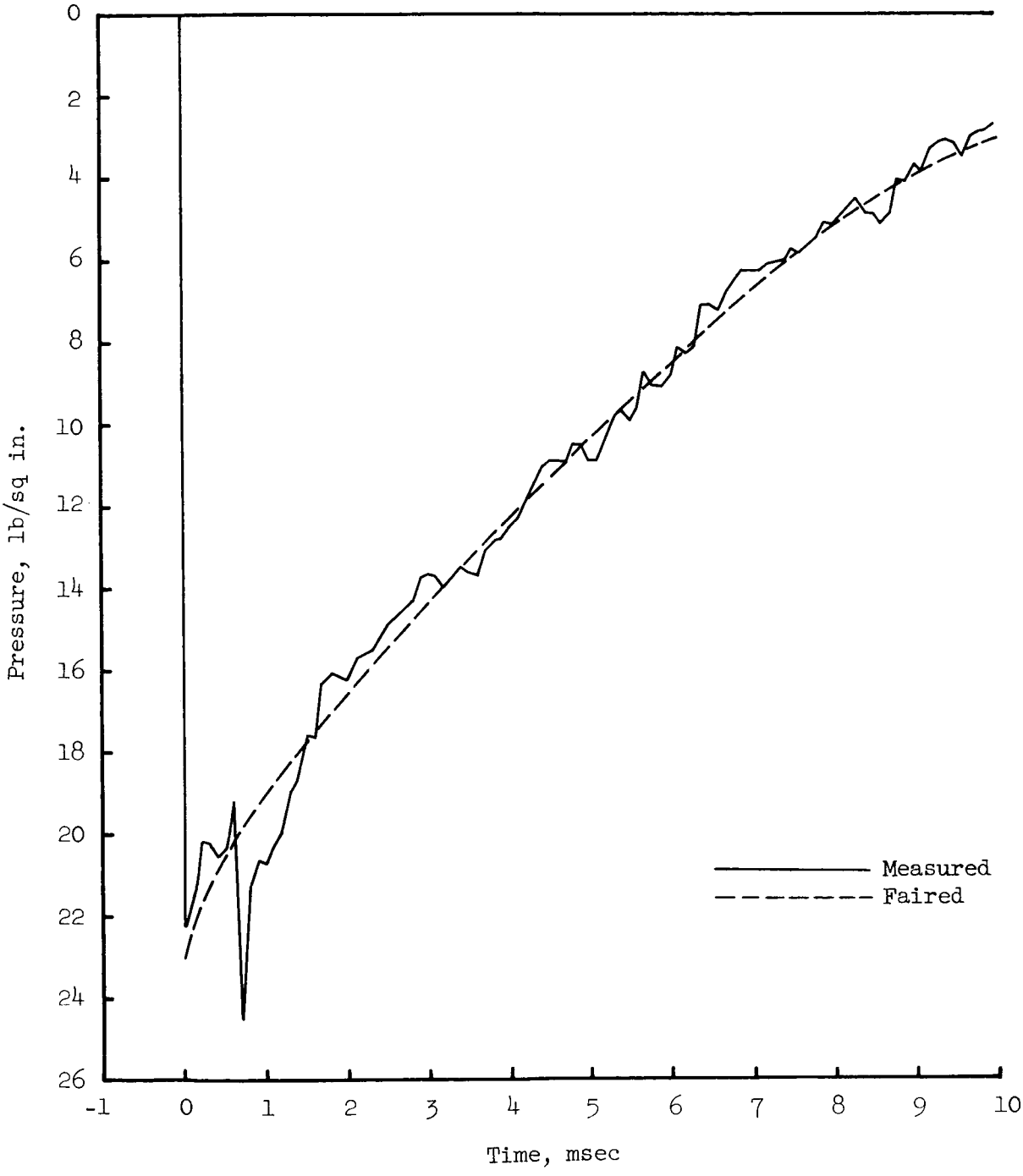

Figure 8.- Pressure time histories at blast-side 22.5-percent-chord station. Test 1.

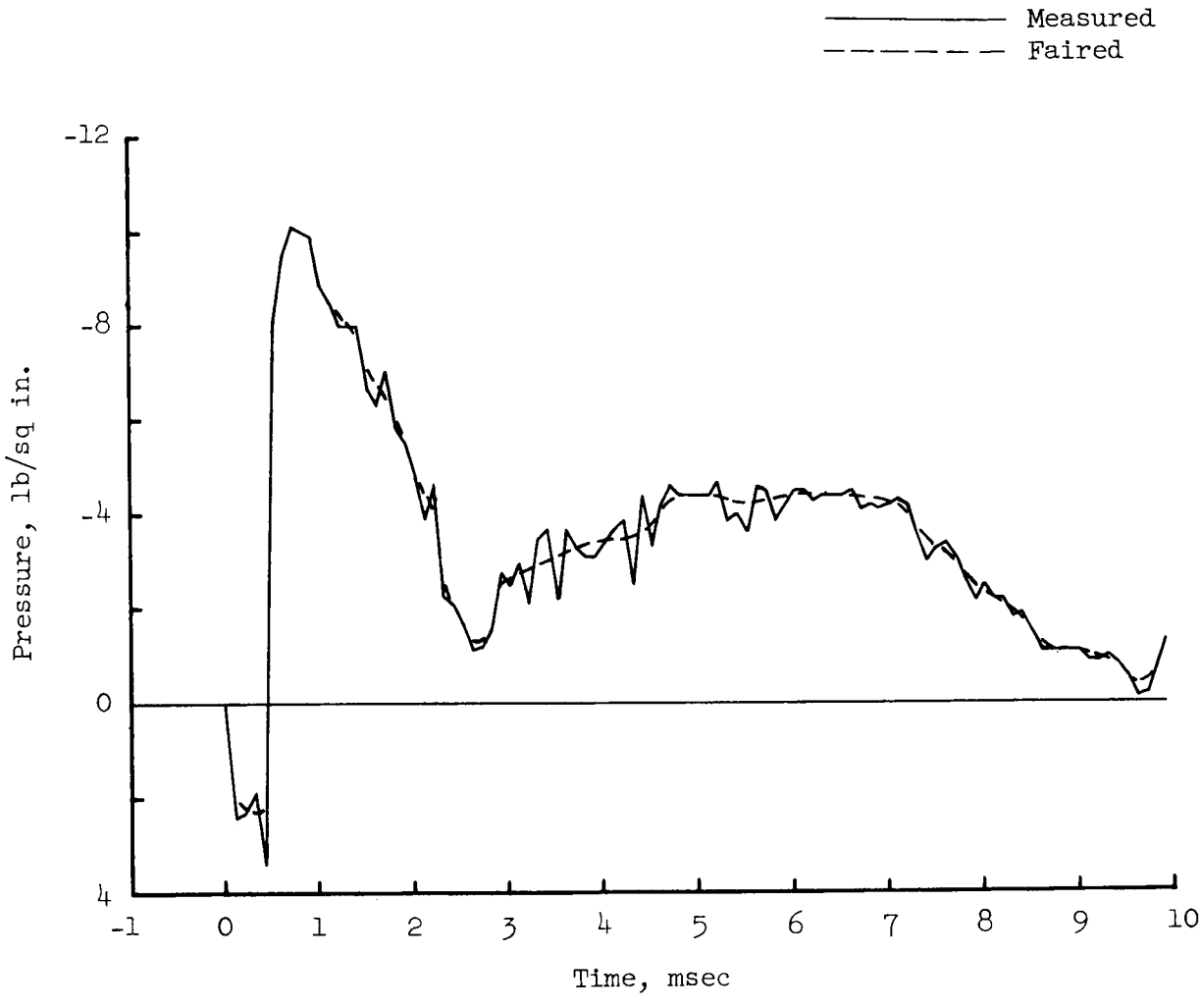

Figure 9.- Pressure time histories at lee-side 15-percent-chord station. Test 1.

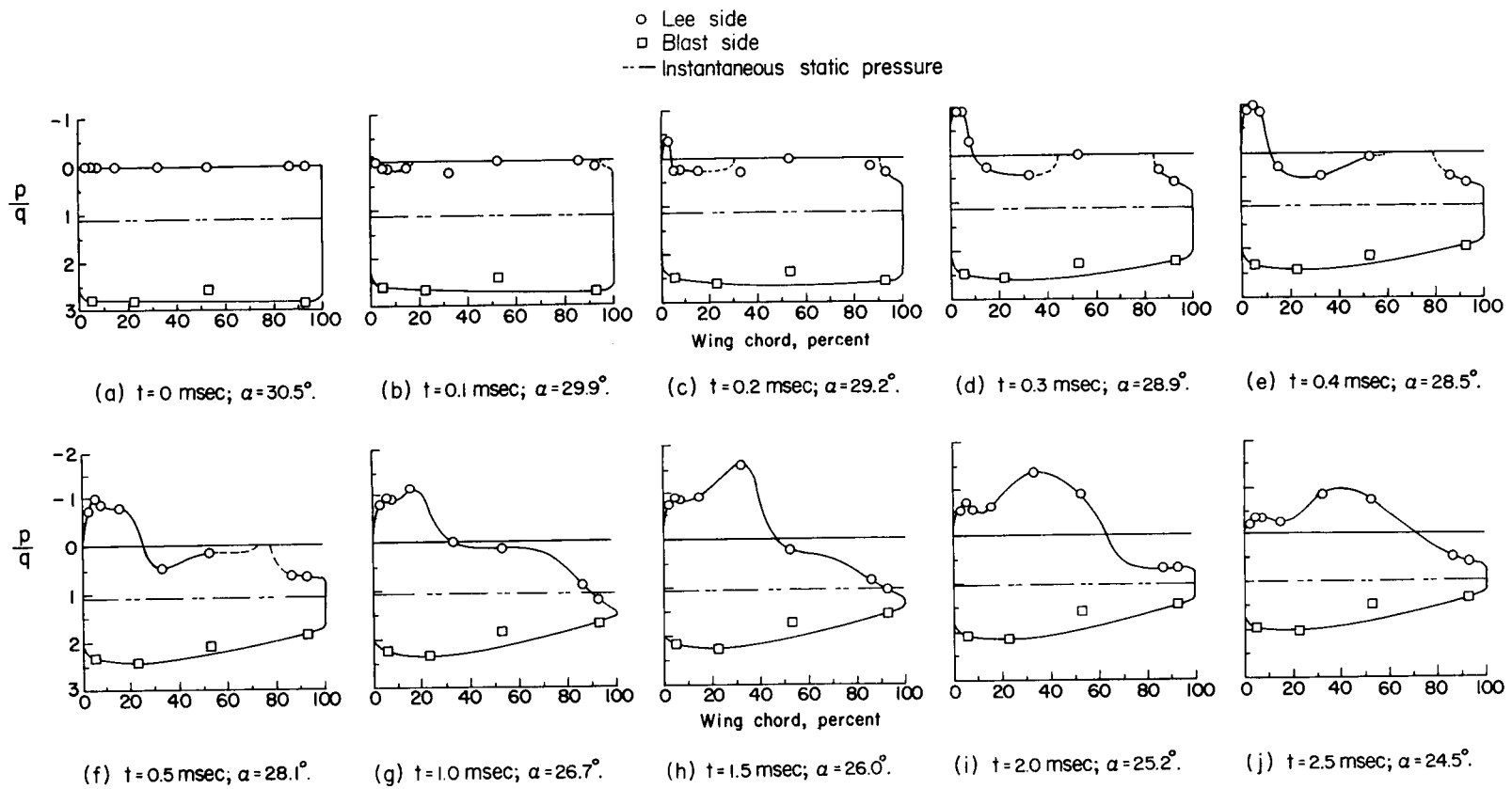

Figure 10.- Chordwise pressure distributions. Test 1.

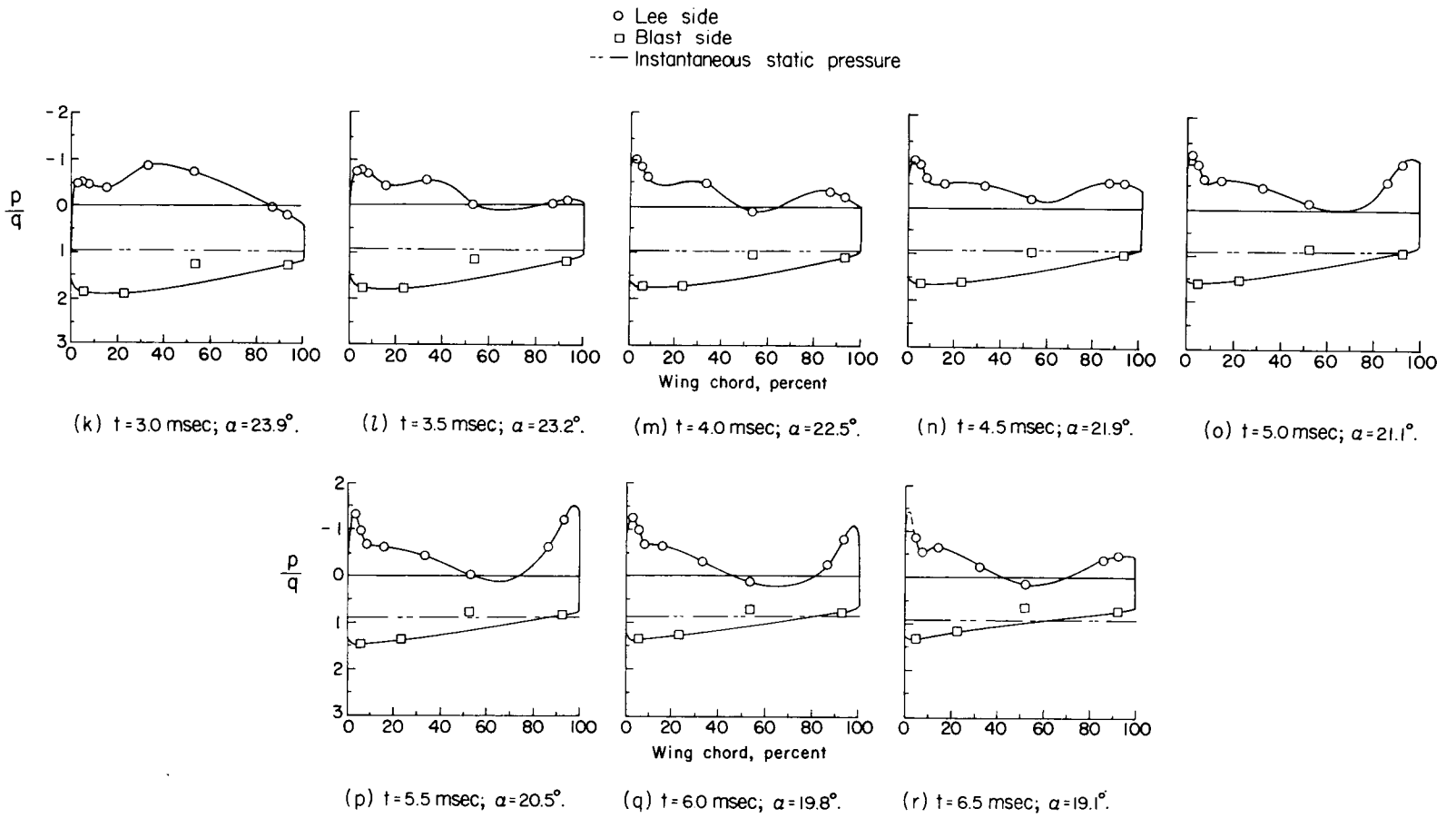

Figure 10.- Concluded.

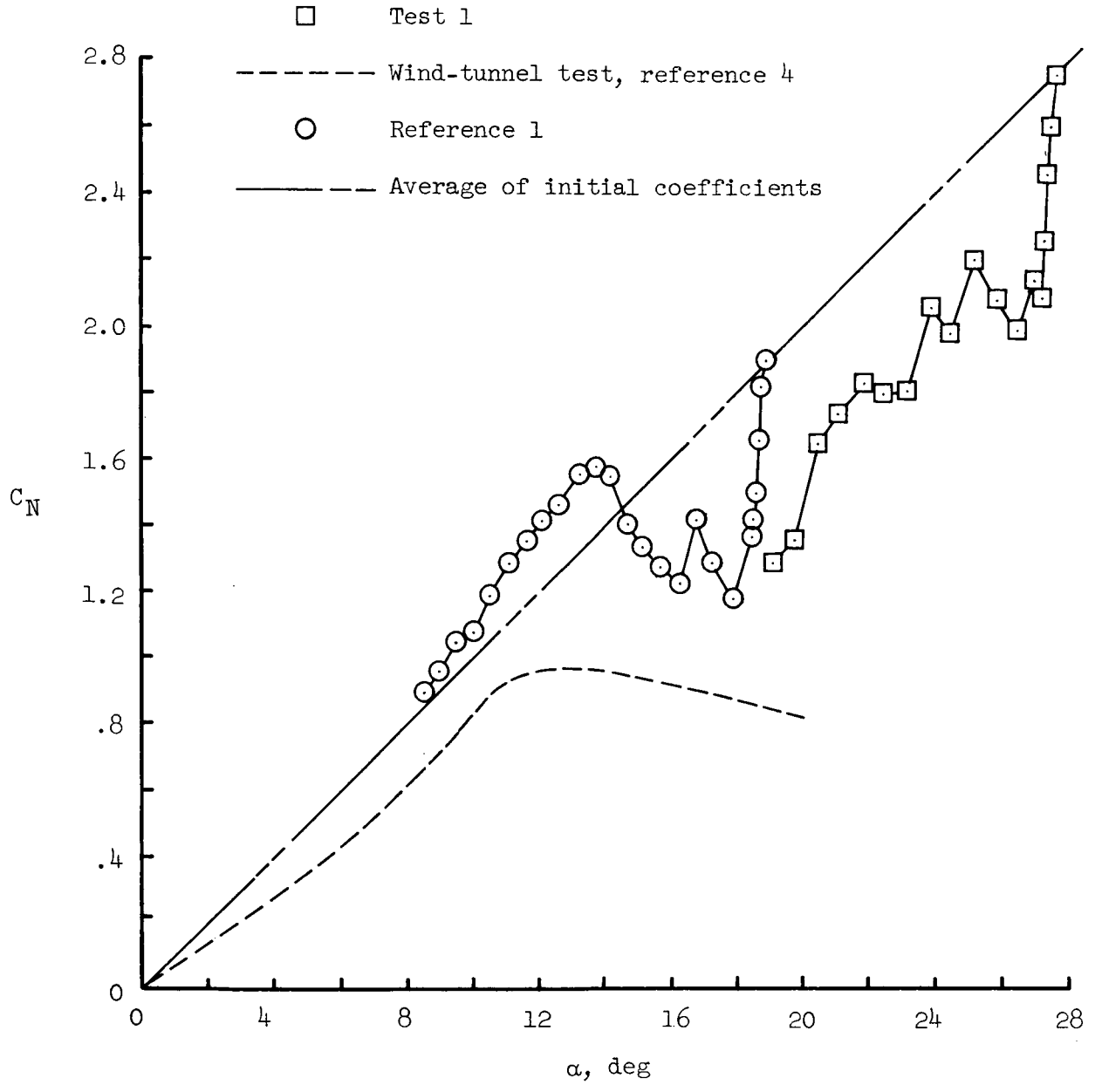

Figure 11.- Comparison of normal-force coefficients obtained from blast and wind-tunnel tests as a function of angle of attack.

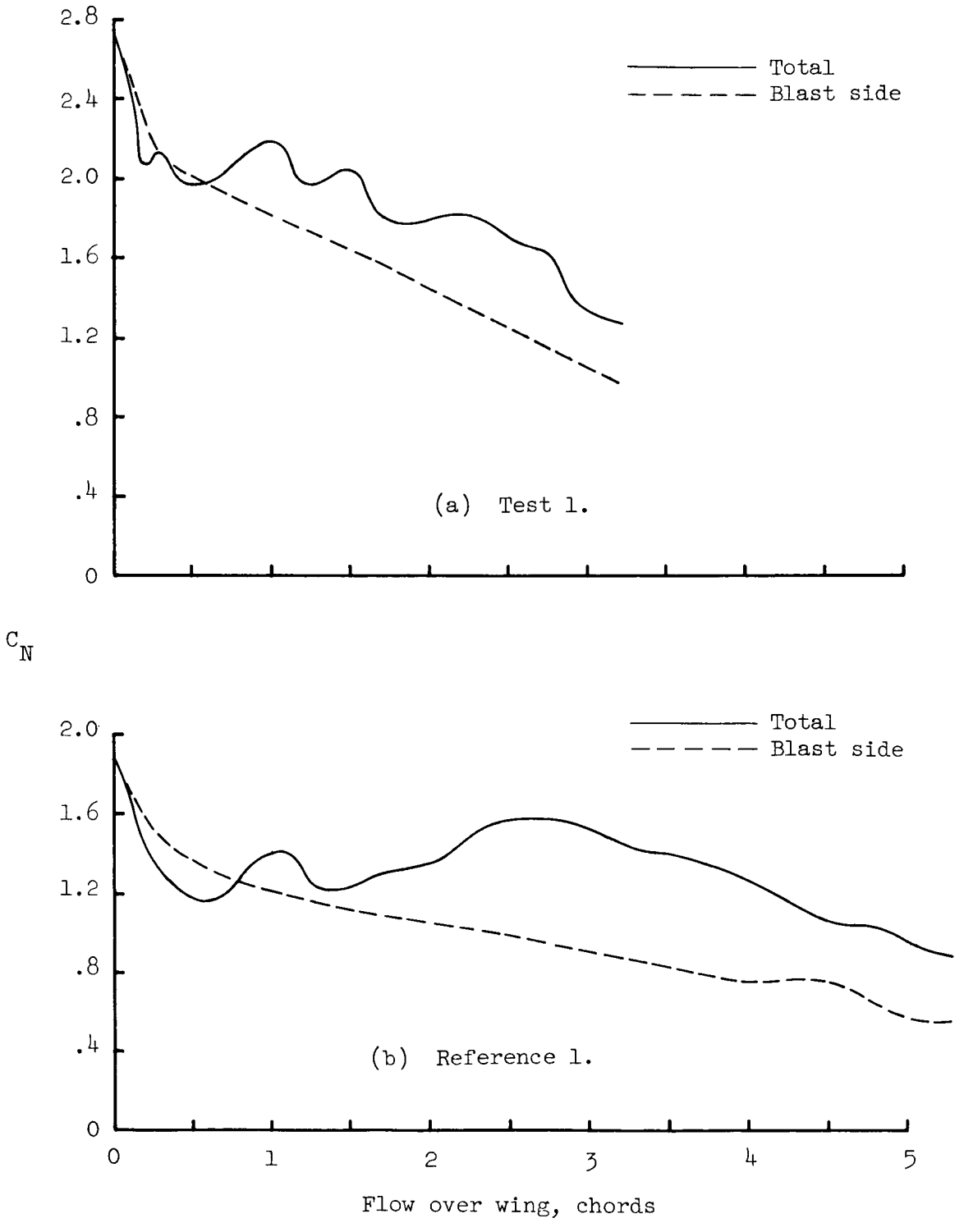

Figure 12.- History of normal-force coefficient.

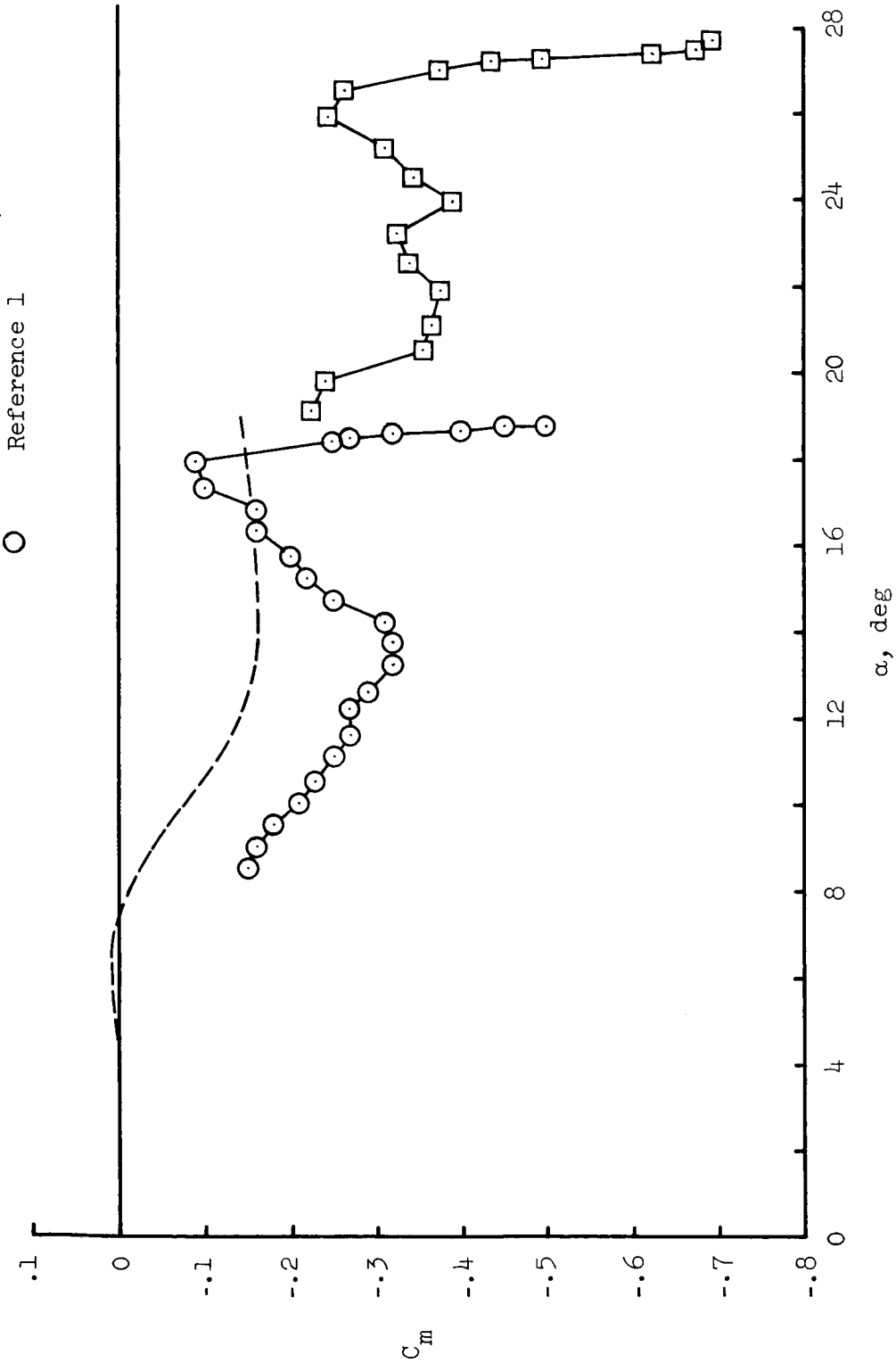

Figure 13.- Comparison of pitching-moment coefficients obtained from blast and wind-tunnel tests as a function of angle of attack.